COMPARISON OF NASCAP MODELING RESULTS WITH LUMPED-CIRCUIT ANALYSIS

David B. Stang and Carolyn K. Purvis
NASA Lewis Research Center

SUMMARY

One of the goals of spacecraft charging studies has been to develop engineering design tools that can be used to predict the development of absolute and differential potentials by "realistic" (i.e., complex in geometry and surface composition) spacecraft under geomagnetic substorm conditions. Two types of analyses are in current use. One is embodied in the NASCAP code, which computes quasi-static charging of geometrically complex objects with multiple surface materials in three dimensions. The second approach is represented by lumped-element equivalent circuit models that have been developed and used by several aerospace corporations for analyses of particular spacecraft. The equivalent circuit models have the advantage of requiring very little computation time. However, they cannot account for effects, such as the formation of potential barriers, that are inherently multidimensional. How much difference does this make in predictions of charging response? The study reported herein provides an answer to this question.

An available charging study for the Defense Satellite Communication System (DSCS-III) spacecraft was used for an equivalent circuit model. This report presents a charging study of this spacecraft made with the NASA Charging Analyzer Program (NASCAP). The spacecraft model is based on the description given in reference 1 and incorporates the material properties given therein. Charging simulation is done in the environment chosen for that study for both equinox and solstice insolation. Steady-state potentials of structure and insulation are compared with those resulting from the equivalent circuit model, and the differences are discussed.

INTRODUCTION

Various computer models have been developed that attempt to predict surface charging of satellites in geosynchronous orbit. Among these are equivalent circuit models (refs. 1 and 2), one-dimensional Langmuir probe models (refs. 3 and 4), and multidimensional codes (refs. 5 to 7). The multidimensional studies have indicated the formation of potential barriers that cut off low-energy secondary and photoelectron emission, allowing the development of negative potentials on sunlit surfaces. By contrast, the equivalent circuit models generally assume that sunlit surfaces are held near space potential by photoemission. What effect do such simplifying assumptions have on the predicted charging response of a spacecraft? Desire for an answer to this question prompted the study reported herein.

This paper compares the charging predictions of an equivalent circuit model with those of a multidimensional code, NASCAP (ref. 5). The DSCS-III spacecraft was chosen for the comparison because an equivalent circuit study performed on it (ref. 1) also provided sufficient description of the spacecraft to allow development of a NASCAP model. The NASCAP model was

designed to represent the dimensions, geometry, and surface material distribution of DSCS-III as closely as possible. Three different sets of material property parameters were used: standard NASCAP properties, "group A" properties, and "group B" properties. Group A properties consist of the values for dielectric constant, thickness, and bulk conductivity specified in the circuit study and standard NASCAP values for all other material property parameters. Group B properties consist of the specified dielectric constant, thickness, and conductivity values plus a set of secondary electron yield parameters contrived to match as closely as possible the yield fractions used in the circuit study.

Although the equivalent circuit model produced only steady-state potentials, which provide the basis for comparison and are the focus of this report, some transient effects seen in NASCAP simulations are noted.

SPACECRAFT MODEL

Geometry

The geometry and dimensions of the DSCS-III satellite and its NASCAP model are illustrated in figures 1 and 2. Areas of various surface materials are listed for both in table I and compared in terms of absolute area and percentage. The NASCAP model is defined in terms of rectangular parallelipipeds, octagons, wedges, flat plates, and booms inside a 17x17x33 grid. The length of each grid cell represents a length of 0.3 meter. Each cell on the model's surface is assumed to consist of some material specified in the object's definition. The surfaces and solar arrays are dotted with cells specified to have conducting surfaces representing the exposed metal typically found on spacecraft.

Two models were devised: one for the dawn condition with the solar array wings oriented as shown in figure 2, and one for the eclipse case with the solar arrays rotated 90^{o} so that they face "Earthward." The solar arrays are represented as flat plates, which must be in orthogonal grid planes. The GDA and MBA antennas are modeled as protruding octagons and rectangles because their shadowing effects and relative size can influence the results.

Materials

The eight materials used for the surfaces of the DSCS-III were modeled in three different ways. First, materials similar to the actual DSCS-III materials were selected from NASCAP's library: "ASTROQUARTZ" for the silica blankets, "SIO2" for OSR's, "SOLAR" for the solar arrays, "NPAINT" (nonconducting paint) for Chemglaze, "ITO" for indium tin oxide, and "ALUMINUM" for the exposed metal. Second, the explicitly defined properties of dielectric constant, thickness, and resistivity, as given in reference 1, were inserted for each material, with all other material parameters remaining standard NASCAP. This set of properties is referred to herein as "group A." Third, the materials' secondary electron yield property parameters were also adjusted in order to reproduce as closely as possible the secondary yields specified in the lumped-circuit study. This set is referred to as "group "B."

The rationale for using these several sets of material properties was to examine different aspects of the charging response of the model. The first set, standard NASCAP, provides a baseline. The group A parameters represent those likely to be chosen by a spacecraft designer using NASCAP. The group B parameters should allow identification of the magnitude of dimensional effects by eliminating as much as possible those effects due to differences in secondary electron yield formulations between NASCAP and the lumped-circuit model.

Parameters for use in the group B property set were devised by using MATCHG, a simple code that incorporates the NASCAP secondary electron yield formulations. MATCHG does a one-dimensional calculation for charging of a single material surface by using a spherical probe approximation in conjunction with a specified Maxwellian (or double Maxwellian) flux. Two secondary electron yield formulations are available: "NORMAL," which calculates yields assuming normally incident primaries; and "ANGLE," which assumes isotropic primaries.

To calculate secondary electron emission from electron impact, NASCAP uses six material properties: four that determine the shape of the curve displaying normalized yield as a function of primary energy; the maximum yield for normally incident primaries, δ_m; and the primary energy at which δ_m occurs, E_m. Backscattered electron yield is calculated by using the atomic number z. Calculation of secondary electron yield due to proton impact as a function of incoming proton energy requires two parameters: primary energy for maximum power loss (designated E_p), and electron yield for 1-keV protons incident. For more discussion of these parameters see, for example, references 7 and 8.

Massaro and Ling's (ref. 1) secondary electron yield coefficients are simply constant fractions indicating secondary electrons out per primary electron or ion. The values given, 0.75 for all dielectrics and 0.50 for all metals, apply to both electron and ion-generated secondaries. These fractions include backscattered as well as "true" secondary electrons. As part of its charging calculations, MATCHG prints out the various current densities to the surface material being charged at various times. In this work the initial values of the current densities were used. For each material the ratio of electron-induced secondary electron plus backscattered electron current densities to incident electron current density was computed and taken as the "yield fraction." The maximum yield was then varied, and the calculation was repeated until the desired yield fraction was obtained (0.75 for dielectrics, 0.50 for metals). Similarly, the ratio of ion-induced secondary electron current density to incident ion current density was computed, and this fraction was adjusted by varying the yield for 1-keV primaries incident. This procedure was followed for each material, for both secondary emission formulations (ANGLE and NORMAL), and produced two sets of group B parameter values per material, either of which generates the proper initial fractions for the secondary yield coefficients. All of this was done by using the same environment to be used in the later NASCAP calculations. The same environment was used because in the NASCAP formulations the yield fractions depend on the environment as well as on the material properties.

Table II summarizes the material property parameter sets (standard NASCAP, group A, group B (ANGLE), and group B (NORMAL)) used for this study. Included are the initial secondary yield fractions for each set of

secondary yield parameters, labeled f_e (electrons) and f_p (protons). Changing the yield fractions can have a significant effect on charging response, as is illustrated in figure 3, where MATCHG's predicted equilibrium potentials are plotted as a function of yield fraction for the optical solar reflector (OSR) properties (see also ref. 8).

Study Description

The plasma environment chosen for this study is that used by Massaro and Ling (ref. 1) for a "severe substorm." It is a single Maxwellian distribution characterized by $kT_e = 7$ keV, $kT_i = 8.8$ keV, $j_{e0} = 0.5$ nA/cm^2, and $j_{i0} = 10$ pA/cm^2. NASCAP requires number densities rather than current densities as input, so conversion was made by the formula

$$n = \frac{j_0}{e}\left(\frac{kT}{2\pi m}\right)^{-1/2}$$

for each species. Number densities were calculated to be $n_e = n_i = 2/\text{cm}^3$. All calculations used this plasma environment definition.

Three different sunlight conditions were investigated: dawn at equinox, dawn at summer solstice, and midnight at equinox. Various combinations of material properties, secondary emission formulation, and insolation were examined; these are summarized in table III. For each case the simulation began with all surfaces at zero potential and was allowed to run for 40 minutes of simulated time to reach equilibrium. By contrast, Massaro and Ling's results (ref. 1) are given as equilibrium potentials hour by hour as the Sun angle changes.

From the standpoint of a hypothetical designer using NASCAP to study charging for this spacecraft, the group A property set seems the logical choice. Given this set of material properties the NORMAL secondary yield formulation represents a "worst case" in a given environment, and the ANGLE formulation represents a "most probable" case. For this study emphasis is on the worst case situation (i.e., NORMAL formulation), but results for the ANGLE case in the dawn equinox condition are also presented for comparison.

RESULTS

Dawn at Equinox

As is evident from table III the dawn-at-equinox case was the most thoroughly examined. It is therefore used as a "baseline" case with which to compare results obtained by using the various sets of NASCAP material parameters, as well as for comparing NASCAP and circuit model results. Differences among NASCAP results with the group A (ANGLE), group A (NORMAL), and group B properties should indicate the influence of secondary electron yields on predicted potentials. Differences between group B and circuit model results should indicate the influence of three-dimensional effects such as potential barrier formation.

As can be seen from table II the secondary electron yield fractions for group A properties with the ANGLE formulation are larger than those for group A properties with the NORMAL formulation. The group B properties

yield fraction for incident electrons (0.75) is between the two group A fractions for most of the insulators. This would lead one to expect the group A (NORMAL) properties to result in the most negative absolute potentials, the group A (ANGLE) properties to yield the least negative absolute potentials, and the group B properties to yield intermediate results. That this is the case can be seen from the summary of steady-state potentials for these cases given in table IV. The table also illustrates the sensitivity of the results to the choice of secondary electron yield parameters and formulation. Clearly the magnitude of the absolute potentials is dramatically affected by the choice of yield formulation. The differential potentials ("deltas") are also strongly affected in magnitude and in some cases also in polarity. In this table and subsequent ones, the insulator potentials listed are for the appropriate insulator cell having the largest differential potential.

Results obtained by using the group B properties are similar to those obtained by using group A (NORMAL); that is, they yield more nearly a worst case than does a nominal set of NASCAP predictions. This is particularly interesting when the NASCAP results are compared with those of the circuit study. From table V and figure 4 it is apparent that, with the exception of the OSR's, predicted absolute potentials from the circuit study resemble those from the group A (ANGLE) calculation much more nearly than those from the group A (NORMAL) or group B calculations. The circuit study's predicted OSR potentials alone are similar to the worst-case NASCAP predictions. There are also notable differences in predicted structure potential. The two worst-case NASCAP calculations yield structure potentials in the range -2 to -3 kilovolts. Even the group A (ANGLE) calculation yields a structure potential of -645 volts, more than three times the circuit study's prediction of -200 volts. This is undoubtedly due to the formation of potential barriers that suppress emission of low-energy secondary electrons and photoelectrons, an effect which NASCAP accounts for but for which the circuit code cannot.

For assessing potentially hazardous areas absolute potentials are of less interest than differential potentials across insulation because the latter represents the electric stress on a material. The differential potentials are listed in tables IV and V as "deltas," and illustrated in figure 4 by the cross-hatched areas. They are somewhat easier to see when plotted separately from the structure potentials, as is done in figure 5. Here it is clear that, despite the similarity in absolute potentials of the OSR's for the circuit study and the worst-case NASCAP calculations, the circuit study predicts a much larger stress on this material (-5.2 kV as compared with -2.8 kV for NASCAP).

On the other hand, both the group A (NORMAL) and the group B NASCAP calculations predict relatively large differentials across the silica cloth composite on the MBA antennas, and across the 570 cloth on the Earth coverage horn, which were predicted by the circuit study to have much lower stresses. The NASCAP values quoted are for shaded portions of these materials and indicate that these are potentially hazardous areas from a charging standpoint that were not identified in the circuit study. NASCAP also predicts much larger differentials for the 527 silica cloth on the north and south panels than does the circuit study.

Dawn: Equinox Compared with Solstice

The circuit study found dramatic differences in the potentials of the south panel's 527 silica cloth and OSR's between equinox and summer solstice conditions of illumination: the south OSR's were at -5.37 kilovolts at equinox and zero volt at solstice, and the 527 cloth was at -0.365 volt at equinox and zero volt at solstice. By contrast, NASCAP predicted only slight differences in the south panel potentials for the two conditions. Table VI summarizes the absolute potentials of the spacecraft and the north and south panel surfaces as computed by NASCAP using group A (NORMAL) and as given by the circuit study. Corresponding differential potentials are illustrated in figure 6. The lack of dramatic change in the south panel potentials between equinox and solstice is evidently a combined consequence of the low Sun angle (67^{o} to the surface normal) and the formation of local potential barriers.

As was the case for equinox the worst-case NASCAP predictions of differential potentials on shaded OSR's are smaller than those from the circuit study, but the silica cloth is predicted to have larger differential potentials by NASCAP.

Midnight at Equinox

The final condition examined was passage into eclipse. For this condition the NASCAP simulation was begun with all surfaces at zero potential in sunlight and continued until equilibrium was reached. Then the Sun was "turned off" to simulate eclipse entry, and the computation was continued until steady state was again attained. Steady-state potentials are given in table VII. The values listed as "before eclipse" for the NASCAP computation are those just before eclipse entry. They are compared to values quoted for a time of 2300 in the circuit study. The values listed as "during eclipse" are NASCAP's equilibrium values (at about 20 min after eclipse entry) and the circuit study's values for a time of 2400. For this condition Massaro and Ling (ref. 1) present potentials only for the structure and the OSR material, which had the largest differential potential.

Results from the two computations are strikingly different. The circuit study results indicate a dramatic change in structure potential in eclipse (-14.16 kV as compared with -240 V in sunlight) and a concurrent dramatic reduction in differential potentials (160 V as compared with -5.16 kV on the OSR's in sunlight). The latter implies that all the insulators have potentials within 160 volts of the structure potential according to this model. The NASCAP calculation (group A (NORMAL)) predicts a larger structure potential in sunlight (-3.03 kV) with smaller differential potential across the OSR's, which is consistent with results from the dawn computations, and a much less dramatic shift in structure potential in eclipse (to -6.98 kV). As is indicated in figure 7 for most materials, the differential potentials are predicted to be smaller in eclipse. There is, however, one striking exception: SOLAR, which is the material used to model the solar array cover slips, has a large positive differential of 1.8 kilovolts. This polarity differential has not been investigated extensively in spacecraft charging studies, but work has been done in conjunction with high-voltage power system studies (e.g., ref. 9). The latter have observed arcing on solar array segments biased so that the

cover slips are positive relative to the interconnects in the presence of plasmas. Although 1.8 kilovolts is not expected to be sufficient to cause such arcing in geosynchronous orbit (5 kV is quoted in ref. 9), such large positive differentials have not been examined for potential charging hazards and thus remain suspect.

TRANSIENT RESPONSE AND SPATIAL VARIATIONS

To this point, all results have been given in terms of steady-state potentials and maximum differential potentials across insulating areas of the spacecraft. In fact, sunlit spacecraft are known to require tens of minutes to attain equilibrium potentials (e.g., ref. 10), and large areas of insulation do not necessarily reach uniform equilibrium potentials. A few interesting temporal and spatial variations that were evident from the NASCAP calculations are discussed in this section.

Figure 8 shows the charging response of several materials and the spacecraft structure for the dawn-at-equinox condition and group A (NORMAL). Here it is clear that the various materials charge at different rates. In a constant environment such as the one used for this calculation, the absolute potentials tend to be monotonic functions of time. However, the differential potentials $\Delta\phi$ across insulation are not necessarily monotonic, as is illustrated in figure 9, where differential potentials for the figure 8 case are plotted. The OSR shows a monotonic $\Delta\phi$, but neither the solar material nor the 570 composite on the MBA antenna does. The differential across the MBA composite early in the simulation is larger than its equilibrium value by about 1 kilovolt. In fact, this was the largest differential potential (-3.8 kV) observed in this study. Thus equilibrium values of differential potential do not necessarily represent a worst case.

Another interesting phenomenon is "overshoot" in absolute potentials of insulating surfaces caused by a sudden change in environment such as entry eclipse. This is illustrated in figure 10, in which the Chemglaze and OSR materials reach absolute potentials more negative than their equilibrium potentials shortly after eclipse entry. In this case differential potentials are maintained at about the pre-eclipse levels during the "overshoot." This type of behavior has been observed in ground-based electron spraying experiments (ref. 11). It is illustrated here to emphasize the point that, even in eclipse, times of the order of tens of minutes may be required for equilibration.

Even in equilibrium, insulating areas are generally not at uniform potentials. The amount of potential variation over an area depends in a complex manner on the geometry, illumination, and material properties of both the insulator in question and the surfaces around it. The complexity of these dependences makes it difficult to generalize. For the worst-case sunlit conditions investigated for this study, typical variations of potential across insulating areas were of the order of 1 kilovolt. Maximum variations, for example, on the MBA composite cloth, were about 2 kilovolts, and minimum variations, on the Chemglaze and OSR's were 100 volts. The 2-kilovolt maximum variations are large enough to suggest the possibility of surface arcing. Figure 11 illustrates the variation in differential potentials with position on the solar array wings for a dawn-at-equinox condition. The solid line (labeled x = 0) represents differential potential along the center of the array; the dashed line (x = 2) represents

differentials along an edge. The potential variations are clearly nonlinear and are steeper and more negative near the body of the spacecraft.

CONCLUSIONS

Based on the results of this study it is believed that, although an equivalent circuit analysis may provide a rough estimate of charging effects, an early design check using NASCAP is warranted. For the case of DSCS-III, the NASCAP analysis raised concerns about charging of the silica composites on the MBA antennas and Earth coverage horn that were not identified in the circuit study. The time-dependent calculation performed by NASCAP provides important information because of the long time required for equilibration and the fact that differential potentials may not be maximum at equilibrium (again the MBA composite provides an example).

Finally, it is noteworthy that one of the authors (David B. Stang) who developed the NASCAP model of DSCS-III and ran all the computer calculations, did so entirely within a 12-week student assignment at NASA Lewis as a summer employee. That he was able to accomplish this helps to substantiate the claim that NASCAP is indeed a user-oriented code.

REFERENCES

1. Massaro, M. J.; and Ling, D.: Spacecraft Charging Results for the DSCS-III Satellite. Spacecraft Charging Technology - 1978, NASA CP-2071, AFGL TR-79-0082, 1979, pp. 158-178.
2. Inouye, G. T.: Spacecraft Potentials in a Substorm Environment. Spacecraft Charging by Magnetospheric Plasmas, A. Rosen, ed., Progress in Astronautics and Aeronautics, Vol. 47, American Institute of Aeronautics and Astronautics, Inc., 1976, pp. 103-120.
3. DeForest, S. E.: Spacecraft Charging at Synchronous Orbit. J. Geophys. Res., vol. 77, Feb. 1, 1972, pp. 651-659.
4. Garrett, H. B.: The Calculation of Spacecraft Potential - Comparison Between Theory and Observation. Spacecraft Charging Technology - 1978, NASA CR-2071, AFGL TR-79-0082, 1979, pp. 239-255.
5. LaFramboise, J. G.; Godard, R.; and Prokopenko, S. M. L.: Numerical Calculations of High-Altitude Differential Charging: Preliminary Results. Spacecraft Charging Technology - 1978, NASA CP-2071, AFGL TR-79-0082, 1979, pp. 188-196.
6. Katz, I.; et al.: The Capabilities of the NASA Charging Analyzer Programs. Spacecraft Charging Technology - 1978, NASA CP-2071, AFGL TR-79-0082, 1979, pp. 101-122.
7. Katz, I.; et al.: A Three Dimensional Dynamic Study of Electrostatic Charging in Materials. (SSS-R-77-3367, Systems, Science and Software; NASA Contract NAS3-20119.) NASA CR-135256, 1977.
8. Purvis, C. K.: Effects of Secondary Yield Parameter Variation on Predicted Equilibrium Potential of an Object in a Charging Environment. NASA TM-79299, 1979.
9. Stevens, N. J.: Interactions Between Spacecraft and the Charged Particle Environment. Spacecraft Charging Technology - 1978, NASA CP-2071, AFGL TR-79-0082, 1979, pp. 268-294.

10. Purvis, C. K.: Configuration Effects on Satellite Charging Response. AIAA Paper 80-0040, Jan. 1980. (Also NASA TM-81397, 1980.)
11. Purvis, C. K.; et al.: Charging Rates of Metal-Dielectric Structures. Spacecraft Charging Technology - 1978, NASA CP-2071, AFGL TR-79-0082, 1979, pp. 507-523.

TABLE I. - AREAS OF SURFACE MATERIALS FOR DSCS-III AND NASCAP MODEL

Spacecraft area	DSCS-III	NASCAP model	Material	DSCS-III	NASCAP model
	Area, m^2			Area, percent of total	
Earth-facing side	5.28	4.86	527 Silica cloth	35.5	37.0
			570 Silica cloth	12.2	11.1
			Composite silica cloth	44.7	48.2
			Indium tin oxide	.07	1.2
			Exposed metal	7.5	5.6
North panel	4.82	5.13	527 Silica cloth	54.8	61.4
			OSR glass	40.0	35.1
			Exposed metal	5.2	3.5
South panel	5.81	5.13	527 Silica cloth	82.9	73.7
			OSR glass	12.4	12.3
			Exposed metal	4.6	5.3
East panel	3.45	3.51	527 Silica cloth	98.6	97.5
			Exposed metal	3.2	2.5
West panel	3.41	3.51	527 Silica cloth	97.5	97.5
			Exposed metal	2.5	2.5
Back side	5.28	4.86	527 Silica cloth	98.7	98.2
			Exposed metal	1.3	1.0
Solar arrays:					
Sun side	12.18	10.8	Solar array coverslips	96.0	91.7
			527 Silica cloth	4.0	3.3
			Exposed metal	----	5.0
Back side	12.27	10.8	Chemglaze	100.0	100.0

TABLE II. - MATERIAL PROPERTY PARAMETER SETS

Property	Material							
	527 Silica cloth	570 Silica cloth	Composite silica cloth	OSR glass	Solar array cover-slips	Chem-glaze	Indium tin oxide	Exposed metal (Al)
Dielectric constant:								
NASCAP	3.8	3.8	3.8	4.0	3.8	3.5	1	1
Groups A and B	1.7	1.9	1.12	4.5	7.0	2.2	2.4	1
Thickness, cm:								
NASCAP	0.028	0.028	0.028	0.013	0.0179	0.005	------	0.10
Groups A and B	0.030	0.068	0.605	0.020	0.0152	0.005	0.305	0.10
Conductivity, mho/cm:								
NASCAP	2.75×10^{-12}	2.75×10^{-12}	2.75×10^{-12}	1×10^{-14}	1×10^{-17}	5.9×10^{-14}	------	------
Groups A and B	1×10^{-13}	1×10^{-14}	1×10^{-14}	1.3×10^{-14}	2.1×10^{-15}	3×10^{-14}	------	------
Atomic number	10	10	10	10	10	5	10	13
Mean atomic weight, amu	1.02	1.02	1.02	1.02	3.15	1.05	------	------
Photocurrent, mA/cm^2	0.02	0.02	0.02	0.02	0.02	0.02	0.032	0.04
Surface resistivity, Ω	1×10^{11}	1×10^{11}	1×10^{11}	1×10^{19}	1×10^{19}	1×10^{13}	------	------
Standard NASCAP and group A:								
Maximum secondary energy for normally incident primary electrons, δ_m	2.4	2.4	2.4	2.4	4.1	2.1	2.205	0.97
Primary energy for maximum secondary yield, E_m	0.4	0.4	0.4	0.4	0.41	0.15	0.335	.3
Initial secondary yield fraction for electrons, f_e:								
ANGLE	0.983	0.983	0.983	0.983	1.28	0.824	1.22	0.679
NORMAL	0.663	0.663	0.663	0.663	0.904	0.412	0.781	0.524
Secondary yield for 1-keV incident protons, δ_p	0.455	0.455	0.455	0.455	0.244	0.455	0.49	1.5
Primary proton energy for maximum power loss, E_p	140	140	140	140	230	140	123	230
Initial secondary yield fraction for protons, f_p:								
ANGLE	3.09	3.09	3.09	3.09	3.10	3.10	0.364	1.19
NORMAL	1.55	1.55	1.55	1.55	1.56	1.56	0.182	0.057

TABLE II. - Concluded.

Property	Material							
	527 Silica cloth	570 Silica cloth	Composite silica cloth	OSR glass	Solar array cover-slips	Chem-glaze	Indium tin oxide	Exposed metal (Al)
Group B (ANGLE):								
Maximum secondary energy for normally incident primary electrons, δ_m	1.54	1.54	1.54	1.54	1.51	3.0	0.409	0.415
Primary energy for maximum secondary yield, E_m	0.4	0.4	0.4	0.4	0.41	0.15	0.335	0.3
Initial secondary yield fraction for electrons, f_e	0.75	0.75	0.75	0.75	0.75	0.75	0.50	0.50
Secondary yield for 1-keV incident protons, δ_p	0.110	0.110	0.110	0.110	0.110	0.110	0.0753	0.0695
Primary proton energy for maximum power loss, E_p	140	140	140	140	140	140	123	230
Initial secondary yield fraction for protons, f_p	0.75	0.75	0.75	0.75	0.75	0.75	0.50	0.50
Group B (NORMAL):								
Maximum secondary energy for normally incident primary electrons, δ_m	3.04	3.04	3.04	3.04	2.99	6.0	0.819	0.823
Primary energy for maximum secondary yield, E_m	0.4	0.4	0.4	0.4	0.41	0.15	0.335	0.3
Initial secondary yield fraction for electrons, f_e	0.75	0.75	0.75	0.75	0.75	0.75	0.50	0.50
Secondary yield for 1-keV incident protons, δ_p	0.220	0.220	0.220	0.220	0.220	0.220	0.151	0.139
Primary proton energy for maximum power loss, E_p	140	140	140	140	140	140	123	230
Initial secondary yield fraction for protons, f_p	0.75	0.75	0.75	0.75	0.75	0.75	0.50	0.50

TABLE III. - CONDITIONS TESTED

Material group	Equinox			Solstice
	Dawn		Midnight (NORMAL)	Dawn (NORMAL)
	NORMAL	ANGLE		
Standard NASCAP	x	x		
Group A	x	x	x	x
Group B	x	x		x

TABLE IV. - DAWN-AT-EQUINOX STEADY-STATE POTENTIALS

Component	Material group					
	A (NORMAL)		A (ANGLE)		B	
	Dawn-at-equinox steady-state potential, kV					
	Absolute	Delta	Absolute	Delta	Absolute	Delta
Spacecraft structure	-2.69	------	-0.645	------	-2.14	-----
North OSR	-5.48	-2.79	-.825	-0.18	-5.05	-2.92
South OSR	-5.44	-2.75	-.825	-.18	-5.05	-2.92
Chemglaze	-3.25	-1.26	-1.47	-.825	-2.94	-.80
Solar array coverslips	-2.39	+.300	-.724	-.079	-1.83	+.31
North panel (527 silica cloth)	-4.17	-1.48	-.821	-.176	-3.55	-1.41
South panel (527 silica cloth)	-3.80	-1.11	-.835	-.190	-3.15	-1.01
East panel	-2.64	+.050	-.514	+.131	-2.22	-.08
West panel	-3.75	-1.06	-.756	-.111	-3.09	-.95
Earth-facing side	-4.49	-1.80	-.561	+.084	-3.93	-1.79
Back side	-3.78	-1.29	-.508	+.137	-3.31	-1.17
MBA (570 silica cloth)	-5.48	-2.79	-.564	+.081	-4.93	-2.79
570 Silica cloth (Earth coverage horn)	-5.54	-2.85	-.502	+.143	-5.06	-2.92

TABLE V. - DAWN-AT-EQUINOX STEADY-STATE POTENTIALS -

COMPARISON WITH CIRCUIT STUDY

Component	Circuit study		Material group					
			A (ANGLE)		B		Standard NASCAP (ANGLE)	
			Dawn steady-state potential, kV					
	Absolute	Delta	Absolute	Delta	Absolute	Delta	Absolute	Delta
Spacecraft structure	-0.20	------	-0.645	------	-2.14	-----	-0.167	------
North OSR	-5.37	-5.17	-.825	-0.18	-5.05	-2.92	-.219	-.052
South OSR	-5.37	-5.17	-.825	-.18	-5.05	-2.92	-.219	-.052
Chemglaze	-1.56	-1.36	-1.47	-.825	-2.94	-.80	-.382	-.215
Solar array coverslips	0	+.200	-.724	-.079	-1.83	+.31	-.20	-.033
North panel (527 silica cloth)	-.365	-.165	-.821	-.176	-3.55	-1.41	-.224	-.057
South panel (527 silica cloth)	-.365	-.165	-.835	-.190	-3.15	-1.01	-.210	-.043
East panel	0	+.200	-.514	+.131	-2.22	-.08	-.122	+.045
West panel	-.365	-.165	-.756	-.111	-3.09	-.95	-.383	-.216
Earth-facing side	-.365	-.165	-.561	+.084	-3.93	-1.79	-.172	-.005
Back side	0	+.200	-.508	+.137	-3.31	-1.17	-.156	+.011
MBA (570 silica cloth)	-.490	-.29	-.564	+.081	-4.93	-2.79	-.150	+.017
570 Silica cloth (Earth coverage horn)	-.420	-.220	-.502	+.143	-5.06	-2.92	-.146	+.021
Indium tin oxide	-.198	+.002	-.645	------	-2.14	-----	-.167	-----

TABLE VI. - COMPARISON OF DAWN STEADY-STATE POTENTIALS

FOR EQUINOX AND SOLSTICE

Component	Equinox		Solstice	
	Group A (NORMAL)	Circuit study	Group A (NORMAL)	Circuit study
	Dawn steady-state potential, kV			
Spacecraft structure	-2.69	-0.200	-2.70	-0.176
North OSR	-5.48	-5.37	-5.44	-5.35
South OSR	-5.44	-5.37	-5.39	0
North panel (527 silica cloth)	-4.17	-.365	-4.15	-.340
South panel (527 silica cloth)	-3.80	-.365	-3.56	0

TABLE VII. - MIDNIGHT STEADY-STATE POTENTIALS AT EQUINOX

Component	Before eclipse				During eclipse			
	Group A (NORMAL)		Circuit study		Group A (NORMAL)		Circuit study	
	Midnight steady-state potential, kV							
	Absolute	Delta	Absolute	Delta	Absolute	Delta	Absolute	Delta
Spacecraft structure	-3.03	------	-0.24	-6.98	------	------	-14.16	-----
OSR	-5.65	-2.62	-5.40	-7.91	-0.930	-0.930	-14.0	+0.16
Solar array coverslips	-2.92	+.110	-----	-5.90	+1.80	+1.80	------	-----
Chemglaze	-4.21	-1.18	-----	-7.36	-.390	-.390	------	-----
East panel	-4.20	-1.17	-----	-7.06	-.080	-.080	------	-----
West panel	-4.25	-1.12	-----	-7.06	-.080	-.080	------	-----

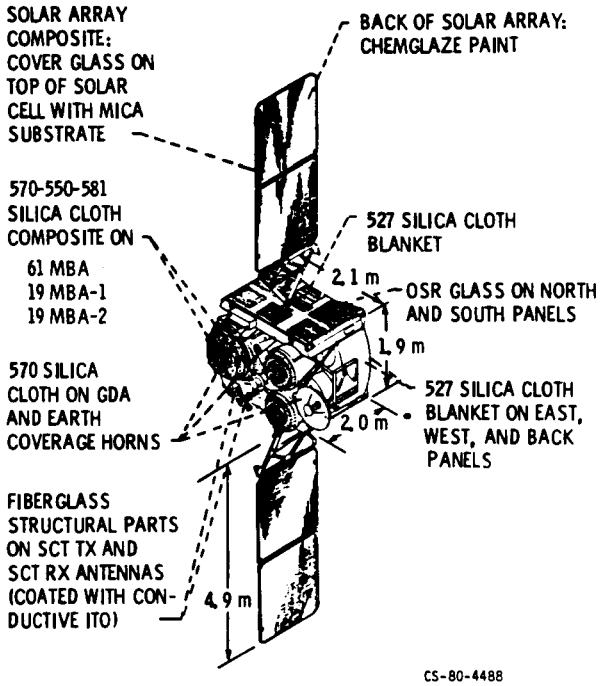

Figure 1. - DSCS-III spacecraft.

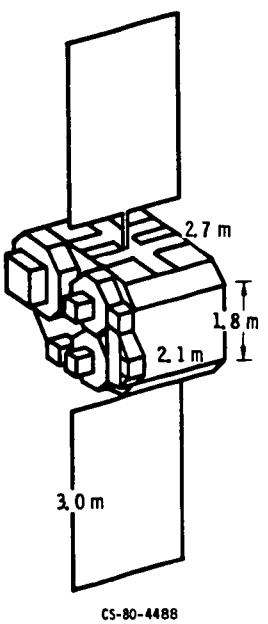

Figure 2. - NASCAP model of DSCS-III.

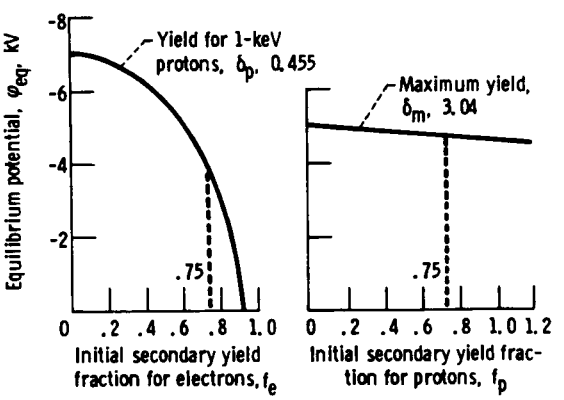

Figure 3. - MATCHG predicted equilibrium potentials as a function of secondary electron yield fraction for optical solar reflectors - NORMAL formulation. Primary energy for maximum secondary yield, E_m, 0.4 keV; primary proton energy for maximum power loss, E_p, 140 keV.

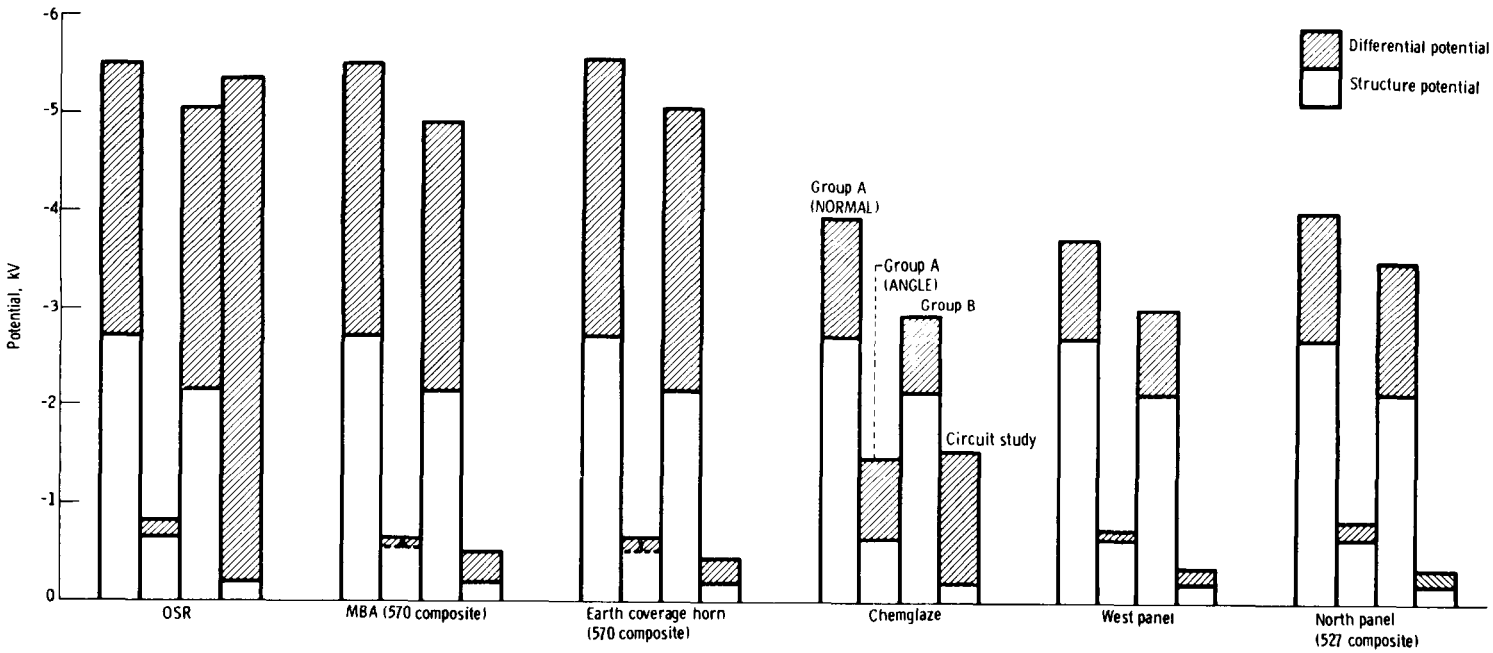

Figure 4. - Dawn-at-equinox steady-state potentials.

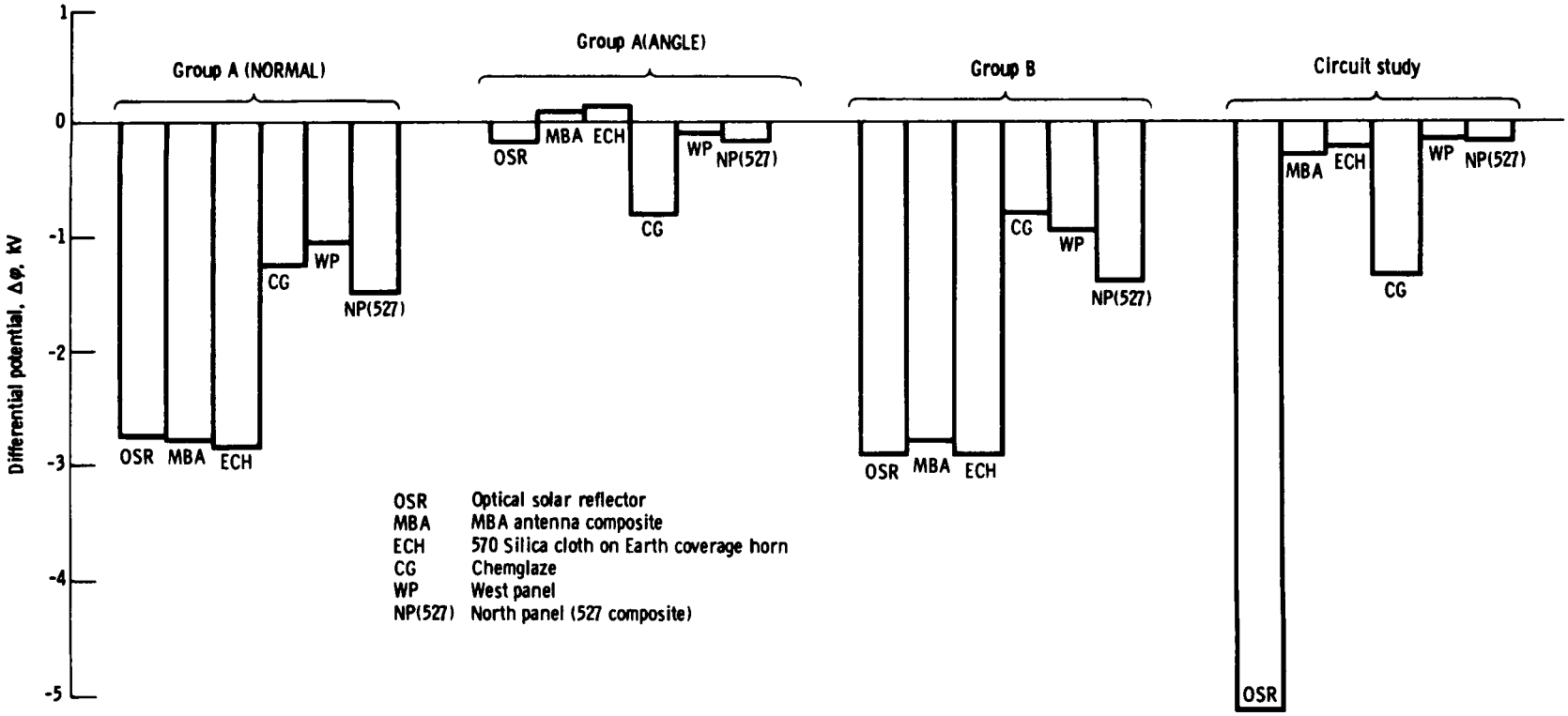

Figure 5. - Dawn-at-equinox differential potentials of selected materials.

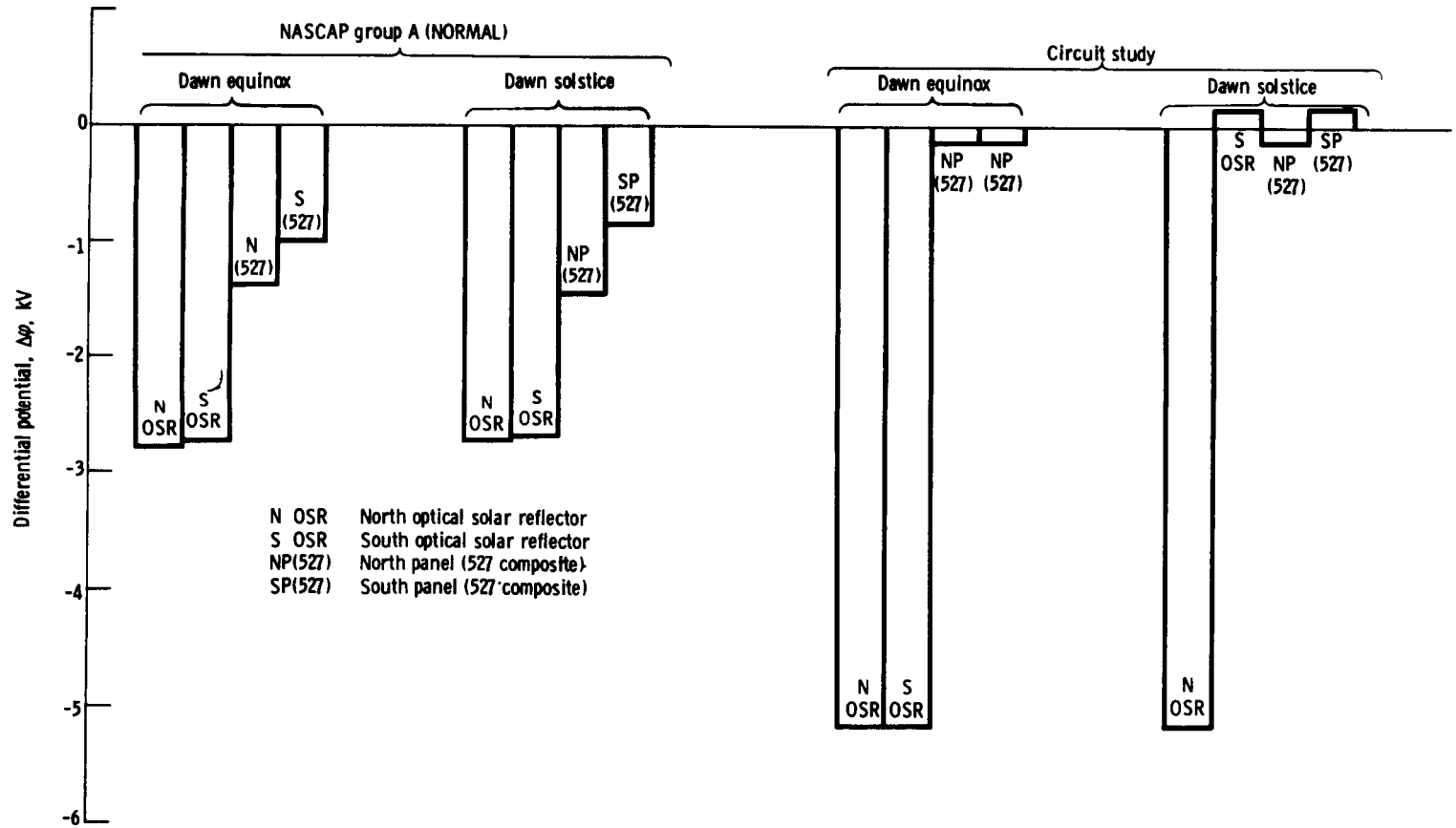

Figure 6. - Dawn differential potentials - comparison at equinox and solstice.

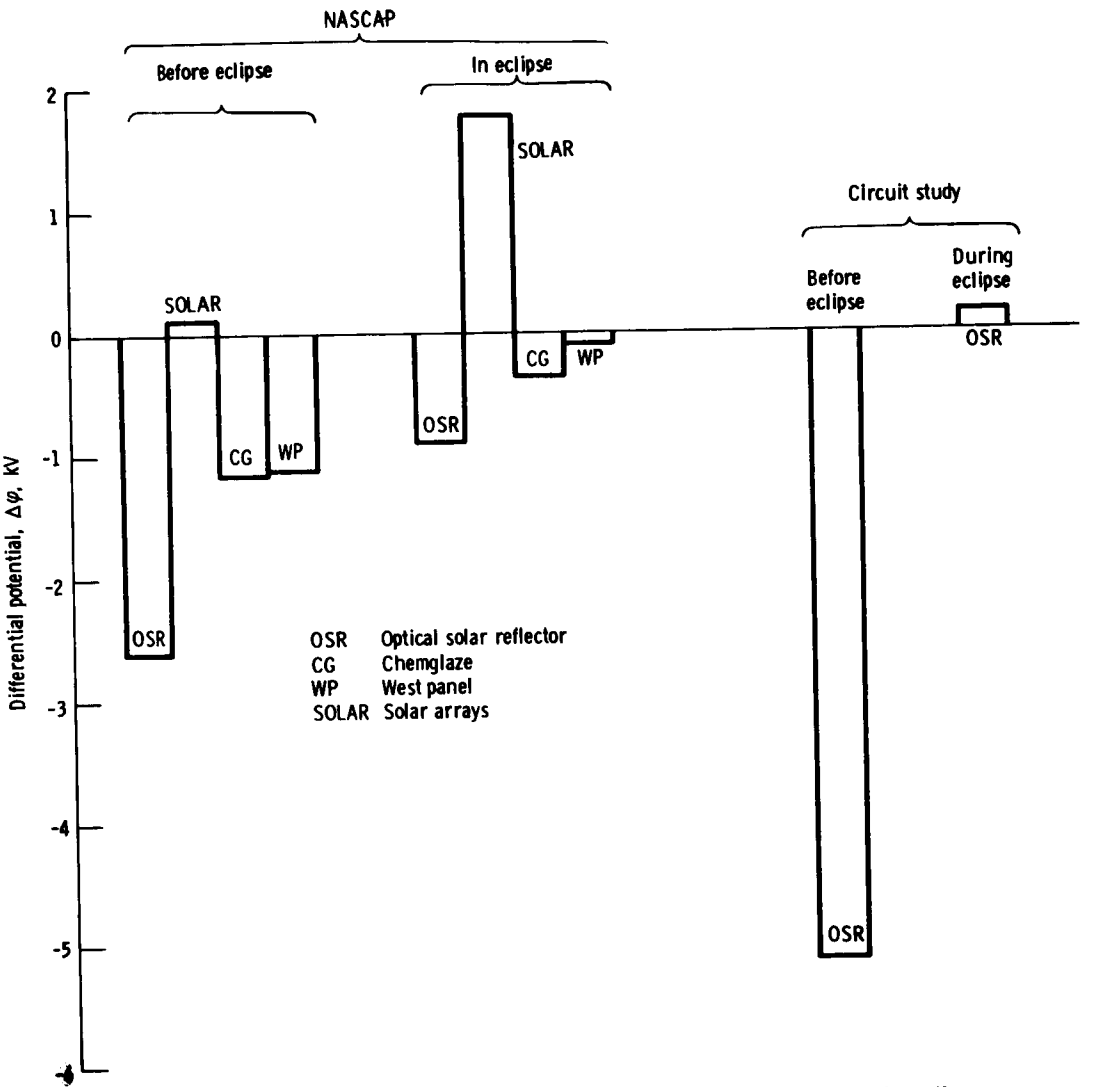

Figure 7. - Midnight-at-equinox steady-state differential potentials before and during eclipse.

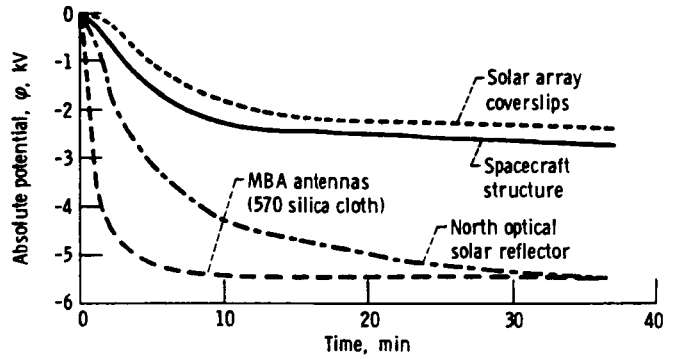

Figure 8. - Dawn-at-equinox absolute potential as function of time for NASCAP group A (NORMAL).

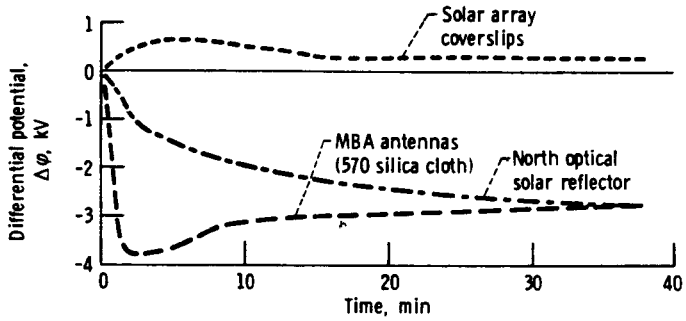

Figure 9. - Dawn-at-equinox differential potential as function of time for NASCAP group A (NORMAL).

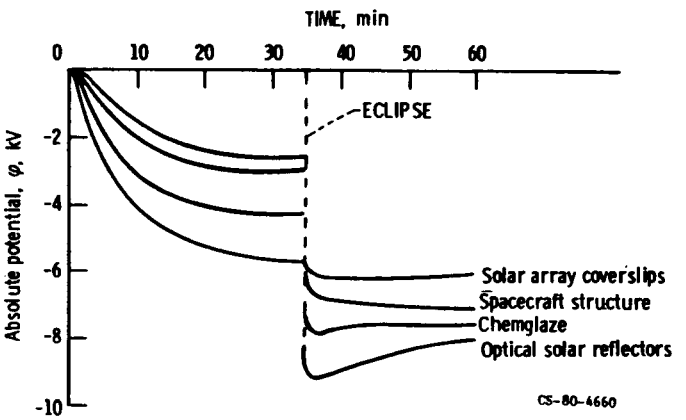

Figure 10. - Midnight-at-equinox potential as function of time for NASCAP group A (NORMAL).